# Enhanced adsorption of polystyrene nanoplastics (PSNPs) onto oxidized corncob biochar with high pyrolysis temperature

Science of the Total Environment

Abdoul Magid, Abdoul Salam Issiaka; Islam, Md Shafiqul; Chen, Yali; Weng, Liping; Li, Jinbo et al

https://doi.org/10.1016/j.scitotenv.2021.147115

Science of the Total Environment 784 (2021) 147115

Contents lists available at ScienceDirect

Science of the Total Environment

journal homepage: www.elsevier.com/locate/scitotenv

# Enhanced adsorption of polystyrene nanoplastics (PSNPs) onto oxidized corncob biochar with high pyrolysis temperature

Abdoul Salam Issiaka Abdoul Magid [a], Md. Shafiqul Islam [a], Yali Chen [a,*], Liping Weng [a,b,*], Jinbo Li [a], Jie Ma [a], Yongtao Li [c,d]

[a] Agro-Environmental Protection Institute, Ministry of Agriculture and Rural Affairs / Key Laboratory of Original Agro-Environmental Pollution Prevention and Control, MARA / Tianjin Key Laboratory of Agro-Environment and Agro-Product Safety, Tianjin 300191, PR China
[b] Department of Soil Quality, Wageningen University, P.O. Box 47, 6700 AA Wageningen, the Netherlands
[c] College of Natural Resources and Environment, South China Agricultural University, Guangzhou 510642, PR China
[d] College of Resource and Environmental Engineering, Jiangxi University of Science and Technology, Ganzhou, Jiangxi 341000, PR China

## HIGHLIGHTS

- Biochar presented strong potential for the adsorption of PSNPs.
- Adsorption capacity of biochar for PSNPs increased with increased pyrolysis temperature and after aging.
- Pore filling, hydrophobic interaction and hydrogen bonding all involved in PSNPs adsorption to biochar.

## GRAPHICAL ABSTRACT

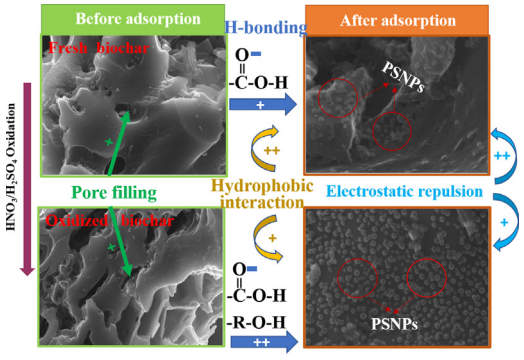


## ARTICLE INFO

*Article history:*
Received 13 January 2021
Received in revised form 18 March 2021
Accepted 9 April 2021
Available online 16 April 2021

Editor: Yolanda Picó

*Keywords:*
Nanoplastics
Corncob
Pyrolysis temperature
Oxidized biochar
Adsorption

## ABSTRACT

Plastic pollution has become a global threat in the natural environment, and an urgent remedial measure is needed to reduce the negative effects caused by plastic pollutants. In the current study, the effects of pyrolysis temperature (500 °C, 700 °C, and 900 °C) and aging on the adsorption of polystyrene nanoplastics (PSNPs) onto corncob biochar were systematically assessed with kinetic, isotherm, pH-dependent adsorption experiments, FTIR and XPS spectroscopy, and DLVO calculations. The oxidation was done with 5% of $HNO_3/H_2SO_4$ to simulate long-term oxidative aging of biochar in the environment. The results showed that the specific surface area, hydrophobicity, and aromaticity of biochar increased with pyrolysis temperature, whereas the specific surface area and amounts of oxygen-containing groups increased after oxidation. The adsorption mechanism of PSNPs onto the biochar was explored based on the correlation between biochar properties and adsorption parameters derived from adsorption isotherms. Overall, the adsorption capacity of biochar for PSNPs increased with increased pyrolysis temperature and after aging. While the increase of specific surface area was considered the major factor leading to the increase of the adsorption, the variation in surface properties also played an important role. Pore filling, hydrophobic interaction, and hydrogen bonding may all be involved in PSNPs adsorption to biochar. However, the hydrophobic interaction might be more important for the fresh biochar, whereas hydrogen bonding involving oxygen-containing groups might make a bigger contribution to PSNPs adsorption to oxidized biochar. The pH experiments revealed that PSNPs adsorption decreased in general with the increase of pH, indicating that electrostatic repulsion played a vital role in the PSNPs adsorption process. The results of this

* Corresponding authors at: Agro-Environmental Protection Institute, Ministry of Agriculture and Rural Affairs, Tianjin 300191, China.
*E-mail addresses:* chenyali@caas.cn (Y. Chen), liping.weng@wur.nl (L. Weng).

https://doi.org/10.1016/j.scitotenv.2021.147115

study indicate that biochar can be potentially applied to immobilize plastic particles in terrestrial ecosystems such as in soil or groundwater, and the immobilization could be enhanced via artificial oxidation or aging of biochar in the natural environment.



## 1. Introduction

Biochar is the pyrolysis product of biomass under a limited amount of oxygen ($O_2$) through the thermal decomposition of organic material (Lehmann and Joseph, 2012). One of the most important properties of biochar is the ability to absorb and retain organic and/or inorganic pollutants (Ahmad et al., 2014; Cao et al., 2011; Chen et al., 2015; Jiang et al., 2012; Koelmans et al., 2006; Li et al., 2020), reducing the bioavailability of environmental pollutants (Alhashimi and Aktas, 2017). Meanwhile, biochar can also benefit soil fertility (Major et al., 2010) and mitigate climate change (Sohi, 2012) at the same time via carbon sequestration.

Many researches have shown that biochar possesses large pore structures, large surface area, surface functional groups (e.g., OH, C—O, C═O, and COOH), as well as various minerals (e.g., N, S, Na, Ca, K and Mg) (Creamer et al., 2014; Ni et al., 2019), and pyrolysis temperature can affect these properties (Kloss et al., 2012). Many studies reported that the pH, aromaticity, specific surface area, and structure stability increased with increasing pyrolysis temperature. In contrast, its hydrophilicity, polarity, and the number of oxygen-containing functional groups decreased (Jia et al., 2018; Mašek et al., 2013). In the environment, biochar would undergo a range of natural "aging" processes, such as oxidation (Cross and Sohi, 2013), biological consumption (Cross and Sohi, 2011), and leaching (Angst et al., 2013), which significantly alter the physico-chemical properties of biochar and further influence its sorption capacity for contaminants. Previous studies have demonstrated that biochar aging is mainly a physical change with structural alterations (Ahmad et al., 2012). However, the change in the surface's chemical properties, such as the increase of oxygen content resulting from aging in biochar (María et al., 2018), can have diverse impacts on biochar affinity for various contaminants. For herbicides (Martin et al., 2012) and phthalates (Ghaffar and Abbas, 2016; Jing et al., 2018), the adsorption efficiency of biochar decreased with aging; while adsorption of dialkyl phthalate on biochar aged with $HNO_3$-$H_2SO_4$ increased, suggesting that the adsorption of phthalates on oxidized biochar surface is a cumulative influence of hydrophobic interactions and pi-pi electron donor-acceptor interactions (Ghaffar et al., 2015).

Nanoplastics are formed from the breakdown of plastic materials, and according to the definition, the size of nanoplastics varies between 1 and 1000 nm and exhibits colloidal conduct (Gigault et al., 2018). Nanoplastics in soil systems have recently received increasing interest (Bläsing and Amelung, 2018; Hurley and Nizzetto, 2018) due to the discovery of their presence in soils worldwide (Scheurer and Bigalke, 2018; Zhang and Liu, 2018), typically resulting from widespread use of agricultural films, sewage sludge and irrigation activities (Bläsing and Amelung, 2018). The small size and high surface area of nanoplastics allow them to pass through biological barriers (Shang et al., 2014), integrate into lipid membranes, affect cellular functions (Rossi et al., 2014), cause mortality (Lee et al., 2013), reduce feeding activity (Wegner et al., 2012), and harm human health (Wright and Kelly, 2017). Nanoplastics have an inhomogeneous charged surface and can aggregate under certain physico-chemical conditions in the environment. Nanoplastics can adsorb organic pollutants (Andrady, 2011) as well as heavy metals (Davranche et al., 2019). Also, nanoplastics can transport in the natural soils (O'Connor et al., 2019; Quevedo and Tufenkji, 2012; Wu et al., 2020) and serve as pollutant carriers to allow the transportation of contaminants that have a more dangerous effect on human and the ecosystem (Da Costa et al., 2016; Wu et al., 2019).

Previous studies focused on studying sources (Duis and Coors, 2016; Nizzetto et al., 2016; Steinmetz et al., 2016), fates (Da Costa et al., 2016; Da Costa, 2019; Hurley and Nizzetto, 2018; Paço et al., 2017), negatives effects (Kashiwada, 2006; Lee et al., 2013; Wegner et al., 2012; Wright and Kelly, 2017) and quantification of nanoplastics (Jiang et al., 2019; Renner et al., 2018; Schwaferts et al., 2019; Strungaru et al., 2019) in the environment. However, there are fewer studies on possible measures to decrease the bioavailability of nanoplastics in the environment and reduce their environmental risks. As previous researches indicated, the biochar filters provide significant capacity for the removal and immobilization of 10 μm microplastic spheres (above 95%) (Wang et al., 2020). Besides, the addition of biochar/$Fe_3O_4$-biochar enhanced deposition of plastic particles due to the increased surface roughness and negatively decreased zeta potentials of porous media (Tong et al., 2020). Thus, the primary objective of this study is to figure out the immobilization ability of fresh and aged biochar for nanoplastics. In this study, corncob was chosen as the feedstock of biochar and pyrolyzed at different temperatures. Meanwhile, fresh biochar was chemically oxidized to simulate the impact of the natural aging process. Polystyrene nanoplastics (PSNPs) was selected because it is an important model for the research of nanoplastics in the laboratory, although the usage and output of polystyrene plastics takes up about 6% of all plastics in the world (Chee et al., 2017). The specific objectives are (1) to obtain qualitative and quantitative information on the adsorption characteristics of PSNPs onto fresh and oxidized biochar, (2) to investigate the environmental pH and pyrolysis temperature effects on the adsorption, and to reveal the involved adsorption mechanisms. This research will broaden our understanding to assess biochar effectiveness in nanoplastics immobilization in water and soils.

## 2. Materials and methods

### 2.1. Preparation of fresh and oxidized biochar

Corncob was obtained from the local farmer in Wuqing District, Tianjin, China. Corncob is a good material for producing active carbon (Ioannidou et al., 2008). The feedstock was air-dried and stored in sealed containers. A slow pyrolizer (CHengYI-1150 °C, High-Temperature Box Furnace, Henan, China) was used to convert corncob into biochar under limited oxygen conditions at 500 °C, 700 °C, and 900 °C (Liu et al., 2014). The temperature increased at 5 °C/min until the required temperature at 500, 700, or 900 °C was reached, and then the peak temperature was maintained for 2 h. Then, the obtained biochar was gently crushed and sieved to <0.15 mm, and referred to as CB500, CB700, and CB900 throughout the manuscript.

$HNO_3$-$H_2SO_4$ mixture was selected to oxidize corncob biochar according to a modified method (Qian and Chen, 2014). Several studies have demonstrated that biochar treated with a strong oxidizing agent (e.g., $HNO_3/H_2SO_4$, $HNO_3$, HF/$HNO_3$, $KMnO_4$, $H_2O_2$, or NaClO) boosts its sorption capacity, creates charged and hydrophilic surface functional groups, and increases their colloidal stability and mobility (Cho et al., 2010). Briefly, the $HNO_3$-$H_2SO_4$ mixture (1:3, v/v) was diluted to 5%, and then 5 g of each biochar sample (CB500, CB700, or CB900) was immersed in 400 mL of $HNO_3/H_2SO_4$ solution. The reaction was strongly exothermic; therefore, the suspension was maintained for 6 h at 80 °C. To eliminate the remaining acid, oxidized biochar was first washed repeatedly with deionized water and then drained through a 0.45 μm membrane. The oxidized biochar samples were denoted as ACB500, ACB700, and ACB900.

### 2.2. Characterization of biochar and PSNPs

Suspensions of biochar were prepared by mixing 0.1 g biochar with 10 mL ultrapure water (Arrium® mini pro-VF Ultrapure Water System). The suspensions were shaken at 250 rpm for 24 h and then centrifuged. The pH in the supernatant was measured with a pH meter (Shen et al., 2018). The ash content of biochar was estimated by weighing the residues of 1.0 g biochar after being heated in a muffle furnace at 750 °C for 6 h (ASTM International, 1984). An elemental analyzer (Vario EL cube SN-19103023) was used to evaluate proportions of carbon, oxygen, hydrogen, nitrogen, and sulfur of biochar through dry combustion. The specific surface area and pore size of small pores (<100 nm) of each biochar were determined using the BET-$N_2$ adsorption technique (Micrometrics Instrument Corporation, TriStar II 3020 Version 3.02 Serial 1421). The pore size of large pores (>100 nm) was determined using the Mercury porosimeter method (Micrometrics Auto Pore IV 9510, USA). The surface morphologies of the materials were observed with a scanning electron microscope (SEM-Hitachi SU-1510). The surface functional groups of biochar were analysed with Fourier transform infrared (FTIR) spectroscopy in the range of 4000–500 $cm^{-1}$ (Thermo Nicolet Corporation, Nexus870). The C and O-containing groups were determined using X-ray photoelectron spectroscopy (Thermo ESCALAB 250Xi XPS Method, USA).

Polystyrene nanoplastics (50 nm) were purchased from Huge Biotechnology, Shanghai, China. The zeta potential and particle size of biochar and PSNPs at pH 4, 7, and 9 were measured using a zeta-potential meter (ZETASIZER Nano Series 1184132, Malvern). The surface functional groups of PSNPs (Fig. S1) were analysed with FTIR in the range of 4000–500 $cm^{-1}$. The pH values of the suspensions were adjusted by adding 0.1 mol/L $HNO_3$ or NaOH. The results of zeta potential and size of biochar and PSNPs are listed in Tables S1 and S2.

### 2.3. Adsorption experiments

#### 2.3.1. Adsorption kinetics

Sorption kinetic studies were conducted to investigate PSNPs adsorption as a function of the contact time to the fresh and oxidized biochar. Briefly, 1 g/L PSNPs solution was prepared as stock solution. 0.2 g of each type of biochar was mixed with 10 mL 0.4 g/L PSNPs solution in a 30 mL glass vial with a Teflon-lined screw cap at 25 °C. The final content of biochar is 20 g/L. The pH of the suspensions was adjusted to 7.0 using 0.01 mol/L $HNO_3$ or NaOH. 30 suspensions were prepared for each biochar. The glasses vials were shaken at 180 rpm on a rotary shaker at room temperature (about 25 °C). At specified intervals (15, 30, 60, 120, 240, 480, 1500, 2160, 2880, and 4320 min), three vials (as triplicates) for each biochar were taken out, and the suspensions were immediately filtered through a 0.45 μm micro-porous filtration membrane for PSNPs analysis. The absorbance value of PSNPs in the filtrate was determined via light absorbance measurement at wavelength of 316 nm using a UV–Vis spectrometer (UV-2700, Shimadzu) (Wegner et al., 2012), and then the PSNPs concentration was calculated using the absorbance value-concentration standard curve (Fig. S2).

#### 2.3.2. Adsorption isotherms

Adsorption isotherms of PSNPs to fresh and oxidized biochar were studied. The experimental procedures are similar to those in the adsorption kinetic experiment. The suspensions contained 20 g/L biochar and PSNPs of varying initial concentrations (0.05–1 g/L), and pH was adjusted to 7.0. The suspensions were shaken for 72 h. Each treatment was carried out in triplicates.

#### 2.3.3. pH dependency of the adsorption

The pH dependency of the PSNPs adsorption to biochar was studied. The experimental procedures are similar to those above. The biochar content was the same (20 g/L), whereas the PSNPs concentration was 0.4 g/L. The pH of the suspensions were adjusted to selected values in the range between 3 and 10. Each treatment was carried out in triplicates.

### 2.4. Data analysis and model fitting

#### 2.4.1. Kinetic and isotherm modelling

The average values for the three replicate samples were used for further analysis. The experimental results of sorption kinetics were analysed by fitting the data to the pseudo-first-order and pseudo-second-order kinetic models. Freundlich and Langmuir models were used to describe the PSNPs adsorption isotherms. All models and the parameters were presented in Supplementary Material S1.

#### 2.4.2. DLVO theory

The DLVO theory explains interactions of particle or colloid to understand the force between surfaces that interact via a liquid medium. In this study, to interpret the adsorption and retention behaviour of PSNPs on biochar, DLVO interaction energies were calculated. The total DLVO interaction energy ($E_{TOT}$) between PSNPs and biochar surface was calculated as a sum of the Lifshitz-van der Waals ($E_{LW}$) and electrical double-layer energy ($E_{EDL}$). The expressions used to calculate the values of $E_{LW}$ and $E_{EDL}$ for the interaction between PSNPs and biochar were given in Supplementary Material S2. The values of the calculated Hamaker constant for the PSNPs–water–biochar is $3.64 \times 10^{-21}$. The calculated DLVO interaction energies were expressed as $kT$, where $k$ is Boltzmann constant, and T is the absolute temperature.

## 3. Results & discussion

### 3.1. Properties of biochar

The element composition, atomic ratio, and ash content of fresh biochar and their oxidized materials are presented in Table 1. The ratios of H/C (0.46–0.28), O/C (0.15–0.12), and (N + O)/C (0.16–0.13) were higher for fresh biochar produced at a lower pyrolysis temperature (500 °C) than at higher temperatures (700 °C, 900 °C), especially the H/C ratio (CB500 about 35% higher than CB700 and CB900, Table 1), indicating relatively lower aromaticity, higher hydrophilicity and higher polarity of CB500 than CB700 and CB900 (Spokas, 2010). With the increasing temperature of pyrolysis, the ratios of H/C, O/C, and (N + O)/C gradually decreased, mainly due to the thermal conversion of organic matter into carbonated organic matter and the formation of structures containing condensed carbon atoms such as aromatic rings (Jing et al., 2018; Qian and Chen, 2014), and a significant decrement was observed between CB500 and CB700 or CB900. For CB700 and CB900, the

**Table 1**
Elemental composition of fresh and oxidized corncob biochar.

| Properties | CB500 | CB700 | CB900 | ACB500 | ACB700 | ACB900 |
|---|---|---|---|---|---|---|
| pH | 9.6 | 9.6 | 9.7 | 3.4 | 3.6 | 3.9 |
| C (%) | 76.80 | 79.90 | 81.20 | 74.70 | 72.90 | 65.30 |
| H (%) | 2.9 | 2.0 | 1.9 | 2.3 | 1.9 | 1.6 |
| N (%) | 1.10 | 0.70 | 0.67 | 2.07 | 1.67 | 1.45 |
| O (%) | 14.90 | 13.90 | 13.70 | 16.97 | 20.29 | 29.26 |
| O/C | 0.15 | 0.13 | 0.12 | 0.17 | 0.21 | 0.34 |
| H/C | 0.45 | 0.30 | 0.28 | 0.39 | 0.31 | 0.29 |
| (N + O)/C | 0.16 | 0.14 | 0.13 | 0.19 | 0.23 | 0.36 |
| Ash (%) | 4.30 | 3.50 | 2.53 | 3.96 | 3.24 | 2.39 |
| SA ($m^2$/g) | 17.8 | 34.5 | 36.3 | 36.9 | 48.2 | 60.8 |
| PV ($cm^3$/g) | 0.04 | 0.06 | 0.06 | 0.09 | 0.11 | 0.13 |
| PS (nm) | 7.31 | 9.12 | 9.79 | 7.07 | 8.82 | 9.09 |
| $Al^{3+*}$ (mg/L) | 0.20 | 0.16 | 0.27 | 0.003 | 0.003 | 0.008 |
| $Ca^{2+*}$ (mg/L) | 1.92 | 2.04 | 2.13 | 0.26 | 0.30 | 1.33 |
| $Mg^{2+*}$ (mg/L) | 3.29 | 7.26 | 9.69 | 0.76 | 0.59 | 1.29 |

SA: Surface area; PV: Pore volume; PS: Pore size
* It is the ion concentration in filtrate of biochar suspensions

differences in elemental composition are small. Oxidation led to an increase of O and N contents, while C and H contents decreased. The O/C ratio increased by 40–70% from 0.13–0.14 to 0.18–0.22 (Table 1) when samples were oxidized with $HNO_3/H_2SO_4$. Similar results have been reported in the literature. For instance, a rise in O/C ratio was found when rice straw and peanut shells biochar were oxidized using $HNO_3/H_2SO_4$ (Ghaffar et al., 2015; Qian and Chen, 2014). The increase of O content (increased by 45–48% in our study, Table 1) of oxidized biochar was mainly resulted from the increase of O-containing functional groups introduced on biochar surfaces (Ghaffar et al., 2015).

Increased pyrolysis temperature enhanced the surface area, pore volume, and pore size of biochar (Table 1). Significant increments were observed between biochar pyrolyzed at 500 °C and those at 700 °C or 900 °C. The specific surface area and small pore (<100 nm) volume of oxidized biochar were much higher than the fresh ones, increased by 39.6–107% and 83.3–125%, respectively (Table 1), but the average size of small pores (<100 nm) decreased after oxidation. The increase of pores (Fig. S3) is possibly caused by the decomposition and consumption of organic matter during the chemical oxidation using $HNO_3/H_2SO_4$ (Ghaffar and Abbas, 2016). On the other hand, the decrease of the average pore size after oxidation might be resulted from the creation of relatively small pores during oxidation. A reduction of average pore size was also observed in peanut shell biochar oxidized with $HNO_3/H_2SO_4$ (Ghaffar and Abbas, 2016). For large pores, each biochar exhibits similar size distribution (average pore size about 2250 nm, Fig. S4). These large pores are probably more dependent on the plant materials and the structure of the biomass rather than the pyrolysis temperature and the oxidation (Hassan et al., 2020). The ash content substantially decreased after oxidation because the alkaline elements were removed when oxidized biochar was washed with water (Qian and Chen, 2014).

### 3.2. Adsorption kinetics

The adsorption of PSNPs to biochar showed a fast-initial adsorption, then slowed down and reached equilibrium within 24 h (Fig. 1). The finding showed that the adsorption occurred in two phases, consisting of a rapid adsorption to the adsorbent surface and a slow adsorption due to probably diffusion of PSNPs into the interior of biochar. Moreover, the first fast phase occurred within 4 h for fresh biochar and 8 h for oxidized biochar, and most (>90%) PSNPs were adsorbed during the fast phase. This process is faster than the adsorption of organic pollutants like diethyl phthalate (DEP) to corncob biochar, for which the equilibrium took 4– 5 days (Jing et al., 2018). The data fitted a bit better with the pseudo-second-order kinetic model ($R^2 = 0.96–0.99$, Table S3) than the pseudo-first-order kinetic model ($R^2 = 0.86–0.97$, Table S3). The values of $k_1$ and $k_2$ (Table S3) increased with pyrolysis temperature for both the fresh and oxidized biochar, whereas $k_1$ and $k_2$ were higher for the oxidized biochar than the fresh one. The variations between the $k_1$ and $k_2$ values were mainly due to differences in the adsorption rate, which were depended on the biochar properties (Bogusz et al., 2015).

### 3.3. Adsorption isotherms

Adsorption isotherms of PSNPs on fresh and oxidized biochar are presented in Fig. 2. The adsorbed amount of PSNPs increased with the increase of initial concentration of PSNPs. The isotherms started to flatten at high concentration. The maximum adsorbed amount (in mg/g) measured followed the order of ACB900 > ACB700 > ACB500 > CB900 > CB700 > CB500. It showed that the adsorption capacity increased after oxidation, whereas the increase of pyrolysis temperature also increased adsorption capacity. This conclusion agrees with several previous studies showing that biochar pyrolyzed at a higher temperature and modified with $HNO_3/H_2SO_4$ increased their maximum adsorption capacity for phthalates (Ghaffar et al., 2015), and aluminium (Qian and Chen, 2014).

The isotherm was fitted using the models of Langmuir and Freundlich (Fig. 2), and the optimized model constants are given in Table S4. The former model is founded on the hypothesis of homogeneous monolayer adsorbate distribution over all the adsorbent surface, containing limited similar sites with equivalent sorption activated energy; the latter assumes multilayer adsorption with heterogeneous sorption surface energy. Both the Langmuir and Freundlich models could well describe the data ($R^2 > 0.9$), with higher $R^2$ for the Langmuir model ($R^2 = 0.97–0.98$, Table S4). When the adsorbed amount is expressed as per unit mass of biochar, the $Q_{max}$ and $K_F$ of PSNPs adsorbed on biochar fitted with the respectively Langmuir and Freundlich models were higher for the oxidized biochar than for the fresh one, indicating higher adsorption capacity on the oxidized biochar. The higher $K_L$ values (0.426, 0.399 and 0.351 L $mg^{-1}$) of ACB900, ACB700, and ACB500 than that for the fresh biochar (0.381, 0.351 and 0.331 L $mg^{-1}$) indicate that the oxidized biochar has a higher affinity for PSNPs than the fresh biochar. The higher affinity in the PSNPs adsorption to ACB900, ACB700, and ACB500 could be attributed to the increase of sites with higher affinity on the oxidized corncob surface, and or to the reduced electrostatic repulsion as a result of higher ionic strength (see below).

Though the increase of pyrolysis temperature and chemical oxidation increased PSNPs adsorption (Fig. 3), this increase is limited considering the much bigger changes in the surface area and pore volume of biochar (Table 1). Take CB500 and ACB900 as an example, between them exists the largest difference in surface area and $Q_{max}$. Compared

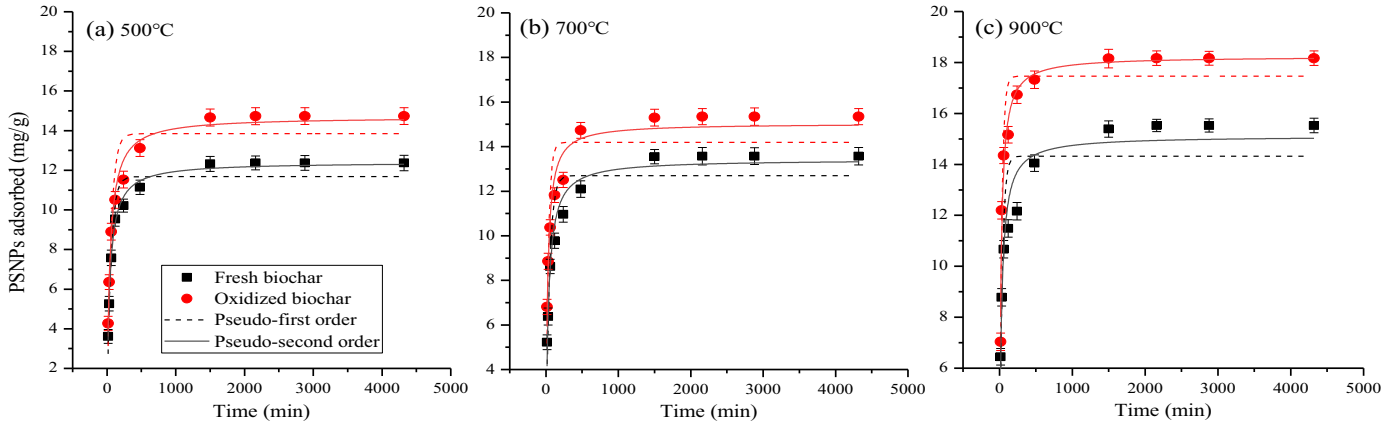


**Fig. 1.** Adsorption kinetics of PSNPs to biochar. Symbols: experimental data. Lines: fitted first-order (dashed line) and second-order (solid line) kinetic models. (a) CB500 and ACB500, (b) CB700 and ACB700, (c) CB900 and ACB900.

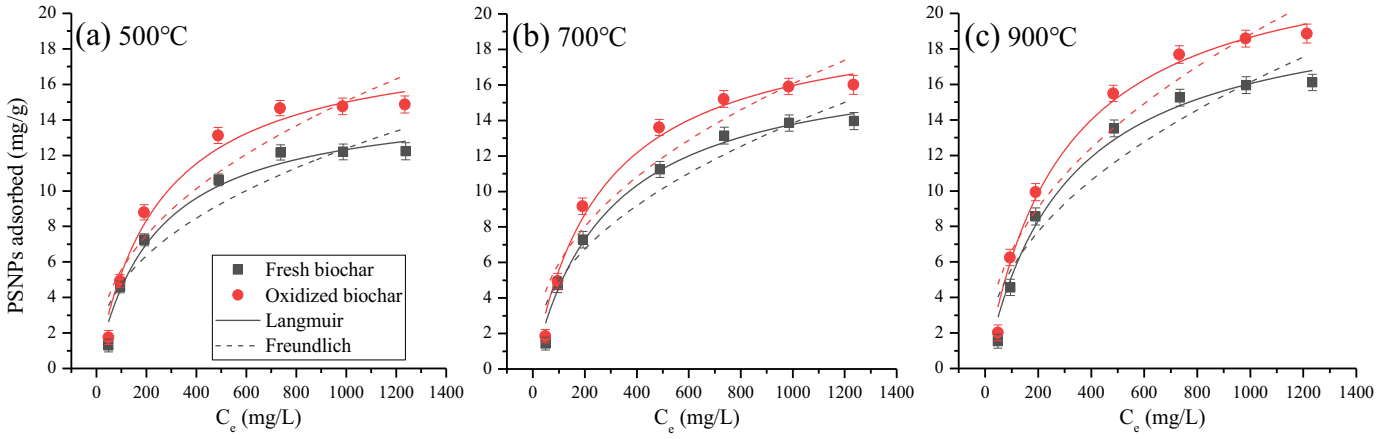


**Fig. 2.** Adsorption isotherms of PSNPs to biochar. Symbols represent the experimental data, and lines represent the modelled results (solid line: Langmuir model; dashed line: Freundlich model). (a) CB500 and ACB500, (b) CB700 and ACB700, (c) CB900 and ACB900.

to CB500, the specific surface area increased 342% in ACB900, whereas the $Q_{max}$ increased only 36.5%. Thus, the increase of PSNPs adsorption is much less than the increase of specific surface area when the pyrolysis temperature was increased, and the biochar was oxidized. When the $Q_{max}$ was expressed in the unit of mg/m$^2$ (Fig. S5), the $Q_{max}$ follows the order of CB500 > ACB500 > CB700 > CB900 > ACB700 > ACB900, exhibiting an opposite trend to that when $Q_{max}$ was based on the mass of biochar. This indicated that the increase of specific surface area might have contributed to the increased adsorption of PSNPs (per unit of mass) on high-temperature pyrolyzed and oxidized biochar. However, the results show that the specific surface area is not the only factor determining PSNPs adsorption to biochar. Due to the size of PSNPs (50 nm), only pores with a size >50 nm can the plastic particles enter. The pores created by the increase of pyrolysis temperature and oxidation are likely small pores (<10 nm, Table 1). These small pores should have contributed significantly to the increase of specific surface area, but due to the size limit PNSPs could not enter into all the pores created, which may be one of the reasons that PNSPs adsorption was not proportional to the specific surface area.

### 3.4. Effect of pH on PSNP adsorption

The pH influences the state of variably charged functional groups and is considered one of the important parameters affecting the adsorption process (Gupta et al., 2018). The effect of pH on PSNPs adsorption to the biochar was investigated by varying the pH from 3 to 10. The results are shown in Fig. 4. In general, for oxidized biochar, more PSNPs were adsorbed at lower pH, and the adsorbed amount gradually decreased with the increase of pH. For the fresh biochar, a maximum adsorption was observed around pH 5, while the adsorption decreased on both sides of pH 5. At lower pH, the protonation of the adsorbent surface reduced the negative charges on surfaces of both biochar and PNSPs (Tables S1 and S2) (Tan et al., 2020; Yang et al., 2019), leading to a relatively decreased electrostatic repulsion between the biochar and PSNPs. When the pH is higher, the negative charge on the biochar surface, and probably on PSNPs also, will rise (Tables S1 and S2), resulting in an increased electrostatic repulsion and less adsorption of PSNPs on biochar. However, there is an opposite pH dependency of PSNPs adsorption to fresh biochar in the pH range 3 to 5 (Fig. 4). The maximum adsorption of PSNPs on fresh biochar adsorbents was at about pH 5 and minimum at pH values about 10. The observed pH-dependent adsorption of PSNPs from 3 to 5 could be attributed to the bridging effect of multivalent cations such as $Al^{3+}$, $Ca^{2+}$, and $Mg^{2+}$ (Table 1) between the fresh biochar and PSNPs. This cation bridging effect is expected to increase with pH due to the increase of interaction between multivalent cations and biochar as well as with PSNPs. However, this effect was a possibility overruled by the increased electrostatic repulsion when the pH increased further above pH 5. This effect of multiple valent cations was absent in the oxidized biochars because the oxidized biochars were washed to remove the acid, resulting in low concentrations of multivalent cations ($Al^{3+}$, $Ca^{2+}$, and $Mg^{2+}$) (Table 1).

### 3.5. DLVO calculations

The DLVO approach is used to describe interaction energies between spherical particles and rough surfaces (Oss, 1993). The total calculations of Lifshitz–van der Waals (LW) and Electrostatic Double Layer interactions (EDL) as a sphere-plate geometry system (Bergendahl and Grasso, 1999) were utilized to predict the adsorption and retention behaviors of the PSNPs on biochar. And the conceptual diagram was put in SI as Fig. S6. The parameters used in the calculation are listed in Tables S1 and S2.

The negative zeta potentials of the PSNPs and biochar under the pH of the experiments decreased with decreasing pH (Table S1), leading to electrostatic repulsion decrement and adsorption increment. Meanwhile, due to the various ions (i.e., $K^+$, $Na^+$, $Ca^{2+}$, $Mg^{2+}$, $Al^{3+}$, $Cl^-$, $F^-$, $NO^{3-}$ and $SO_4^{2-}$) dissolved in the solution at different pH, biochar suspensions had an ionic strength in the range of 0.017 to 0.036 mol/L for fresh biochars and 0.023 to 0.048 mol/L for the oxidized biochars. The relatively high ionic strength for the oxidized biochar can be explained by the presence of $Na^+$ ion when NaOH was added to adjust the pH of the biochar oxidized by acid. High ionic strength, observed in solutions with biochar oxidized and pyrolyzed at a higher temperature, could decrease repulsion between PSNPs and biochar, which is consistent with the higher adsorption affinity of oxidized biochar and biochar with higher pyrolysis temperature (Table S4). In Fig. 5, the DLVO calculation results showed that fresh biochar (18.29 to 44.86 *k*T) had a slightly higher maximum energy barrier than the oxidized ones (18.02 to 43.92 *k*T). For both the fresh or oxidized biochar, the magnitude of the primary energy barrier increased along with the increase of pH, a decrease of pyrolysis temperature, and decrease of ionic strength. These calculated results are in line with the experimental observations regarding the effect of oxidization, pyrolysis temperature, pH, and ionic strength on PSNPs adsorption to biochar, as well as the effects of pH and ionic strength on PSNPs transport in natural soils (Wu et al., 2020). At pH 4 (Table S5), the interaction energy of PSNPs-biochar could readily exceed the relatively low primary energy barrier (18.29 to 16.37 *k*T for fresh biochar and

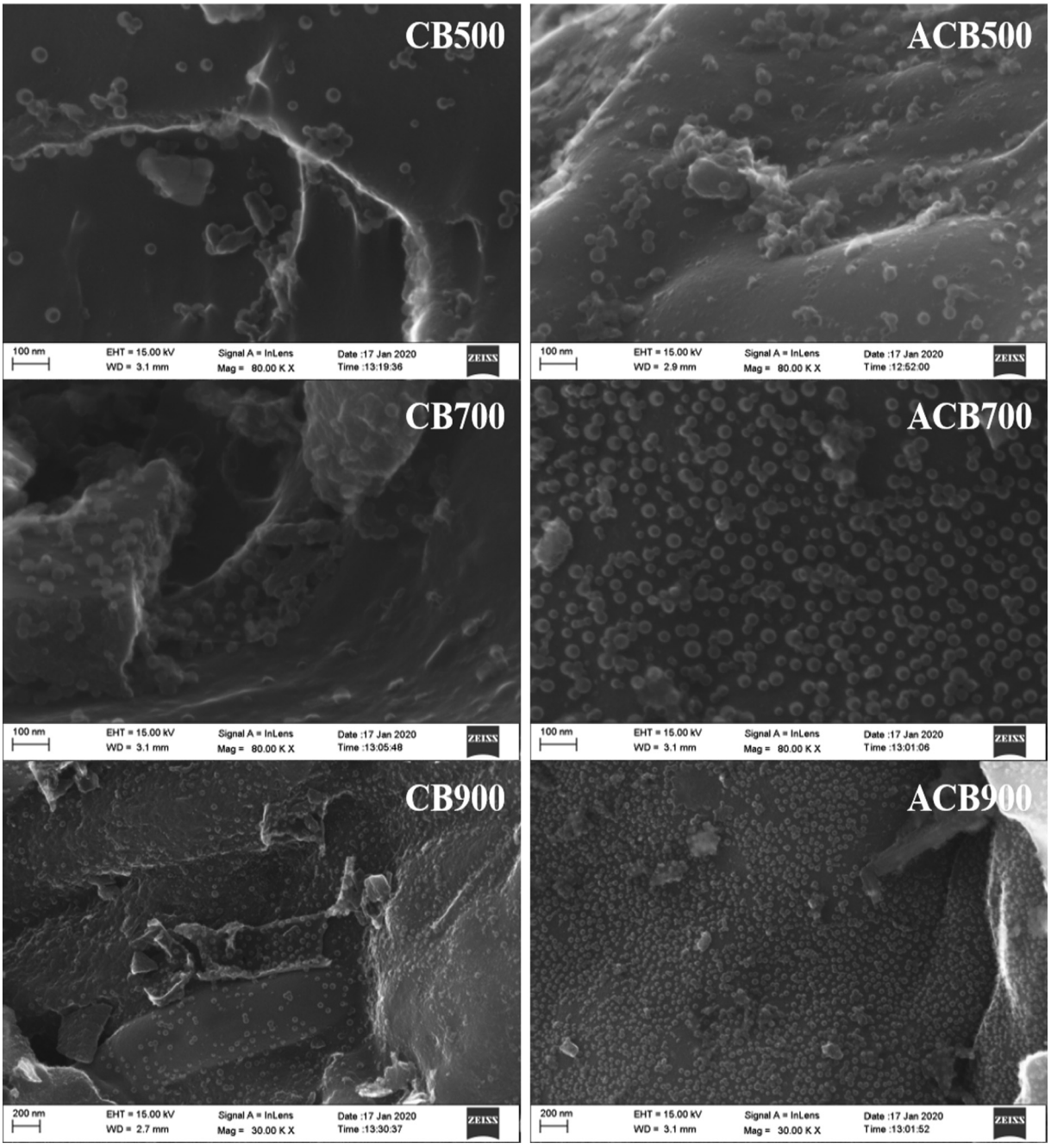


**Fig. 3.** SEM of fresh (CB500, CB700 and CB900) and oxidized (ACB500, ACB700 and ACB900) biochar after PSNPs adsorption.

18.02 to 15.84 *k*T for oxidized biochar) along with the relative stronger van der Waals attraction than at higher pH. Thus, PSNPs could irreversibly deposit into the primary energy minimum. However, at pH 9, with gradually increased primary energy barrier (37.30 to 44.86 *k*T for all biochar) and decreased attraction, it was more difficult for PSNPs to deposit into the primary energy minimum and led to less sorption. Thus, weaker electrostatic repulsion between PSNPs and biochar was responsible for more retention of PSNPs at higher pyrolysis temperature, higher ionic strength, and lower pH. The reversed pH dependency of PSNPs adsorption to fresh biochar between pH 3–5 could not be explained by the current analysis with the DLVO theory. As discussed above, cation bridging may be the mechanism to explain this observation, which was not considered in the DLVO analysis.

### *3.6. Carbon and oxygen-containing functional groups on the biochar surface before and after PSNP adsorption*

Fourier Transform Infra-Red Spectroscopy (FTIR) analysis was carried out to show functional groups present on the biochars (Fig. 6). For fresh biochar, major bands occurred at the wavelength of 3429, 2923, 1743, 1590, 1102 $cm^{-1}$, designated to the stretching vibration of —OH, $CH_2$ (Han et al., 2017), C═O (Jing et al., 2018), C═C (Shen et al., 2018) and C—O—C (Han et al., 2017), respectively. And the peak at 670 $cm^{-1}$ was probably related to C—H (Luo et al., 2018). When the pyrolysis temperature increased, the band intensity at 3429 $cm^{-1}$ (—OH), 1750 $cm^{-1}$ (C═O), 1590 $cm^{-1}$ (C═C), and 670 $cm^{-1}$ (C—H) decreased due to the thermal destruction of cellulose, aliphatic alkyl groups, and aromatic carbonyl and hydroxyl groups (Qian and

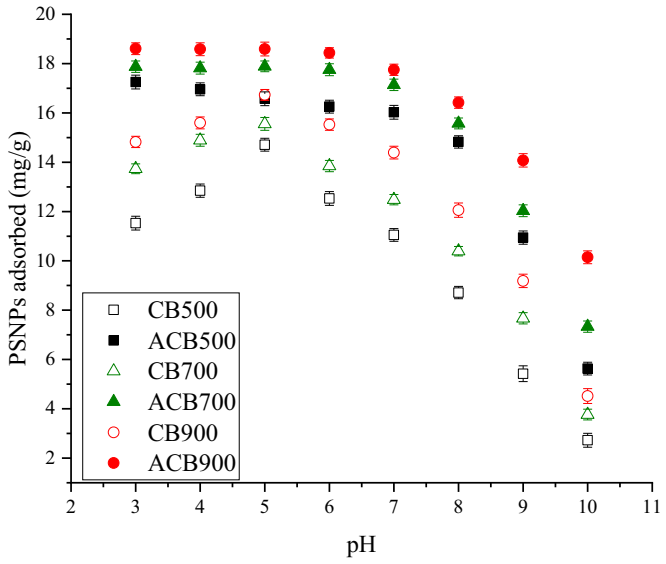


**Fig. 4.** Effect of pH on PSNPs adsorption on biochar.

Chen, 2013). After oxidation by $HNO_3/H_2SO_4$, the intensity of the band increased at 3429 $cm^{-1}$ (—OH), 1750 $cm^{-1}$ (C═O), and 1102 $cm^{-1}$ (C—O—C), indicating an increase in oxygen containing groups on the oxidized biochar surface, especially for ACB700 and ACB900 (Uchimiya et al., 2012). Compared to the bare biochar, after PSNPs adsorption, the band at 3429 $cm^{-1}$ (—OH) and 1102 $cm^{-1}$ C—O—C (Han et al., 2017) decreased significantly. This phenomenon suggests that hydroxyl functional group might play an essential role in the adsorption of PSNPs on biochar due to hydrogen bonding formation, further explaining the higher adsorption of PSNPs on oxidized biochar than fresh ones. Similar hydrogen bonding was also formed between PSNPs and goethite, contributing to higher adsorption of PSNPs on goethite than magnetite (Zhang et al., 2020). The decrease of the ether group (C—O—C) after PSNPs adsorption might be explained by hydrophobic interaction between biochar and PSNPs, because C—O—C groups are nonpolar.

Due to the better PSNPs adsorption ability of biochar at 900 °C pyrolysis temperature, X-ray photoelectron spectroscopy (XPS) characterization was applied to CB900 and ACB900 after and before PSNP adsorption to further identify the dominant C and O functional groups. As shown in Fig. 7, three peaks were located at C1s, i.e., C—C at 284.7 eV, C—H at 284.8 eV, and C—O at 285.4 eV (Jing et al., 2018), and four peaks at O1s, including C═O at 531.15 eV, O—H or C—OOR at 532.5 eV, C═O at 533.2 eV, and C—OOR at 534.0 eV (Fan et al., 2018; Qian and Chen, 2014). There was a decline in C—H and C—C peaks in oxidized biochar and an increase in C—O peak with oxidization (Fig. 7), which was compatible with the compositional data and FTIR results that oxidative aging introduced more O-functional groups onto biochar surfaces. After PSNPs adsorption, the C—C percentage on the biochar surface increased, whereas C—H and C—O declined (Fig. 7), which was consistent with the FTIR results (Fig. 6). Moreover, significant decrement (by ~49%) and increment (by ~75%) were observed for —COOR (carboxyl

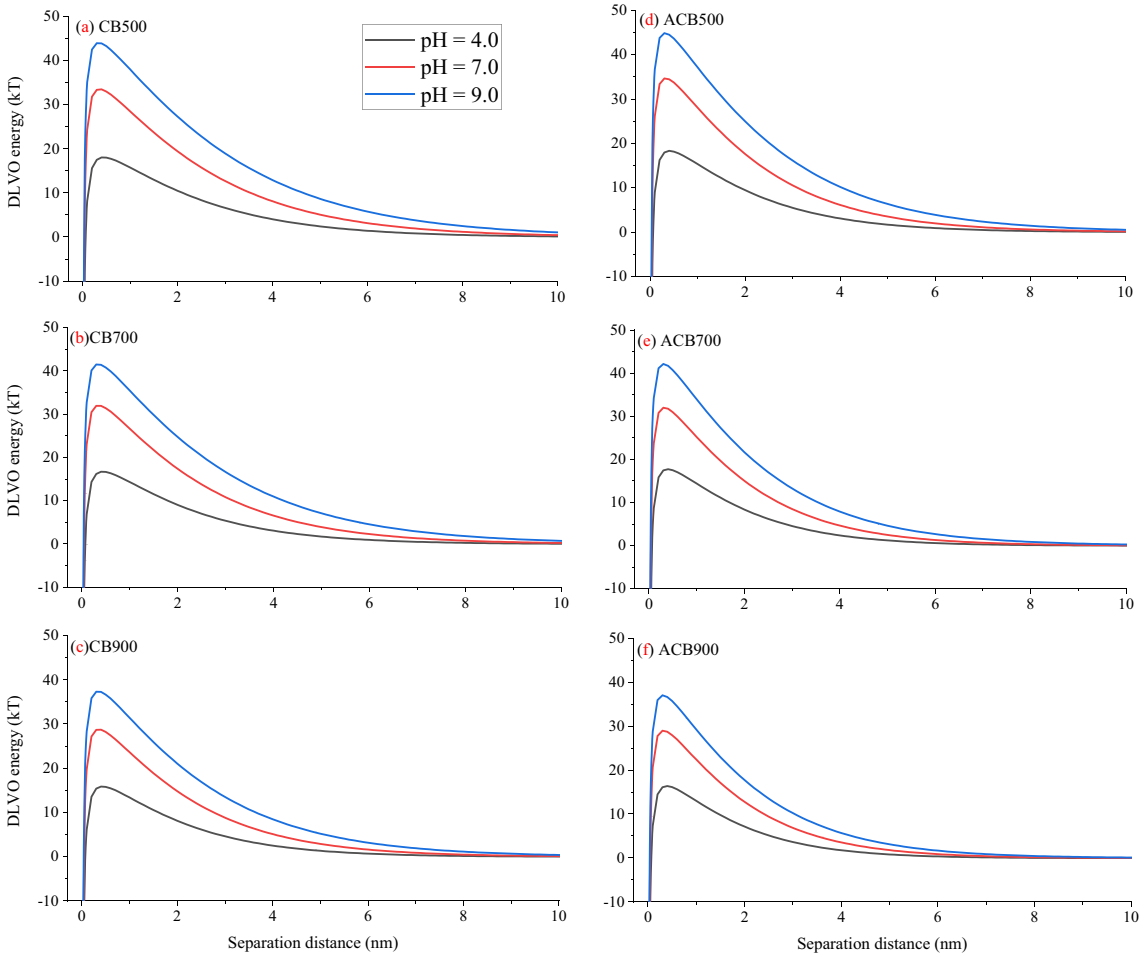


**Fig. 5.** Effect of pH on DLVO force between PSNPs and fresh (CB500, CB700, and CB900) or oxidized (ACB500, ACB700, and ACB900) biochar.

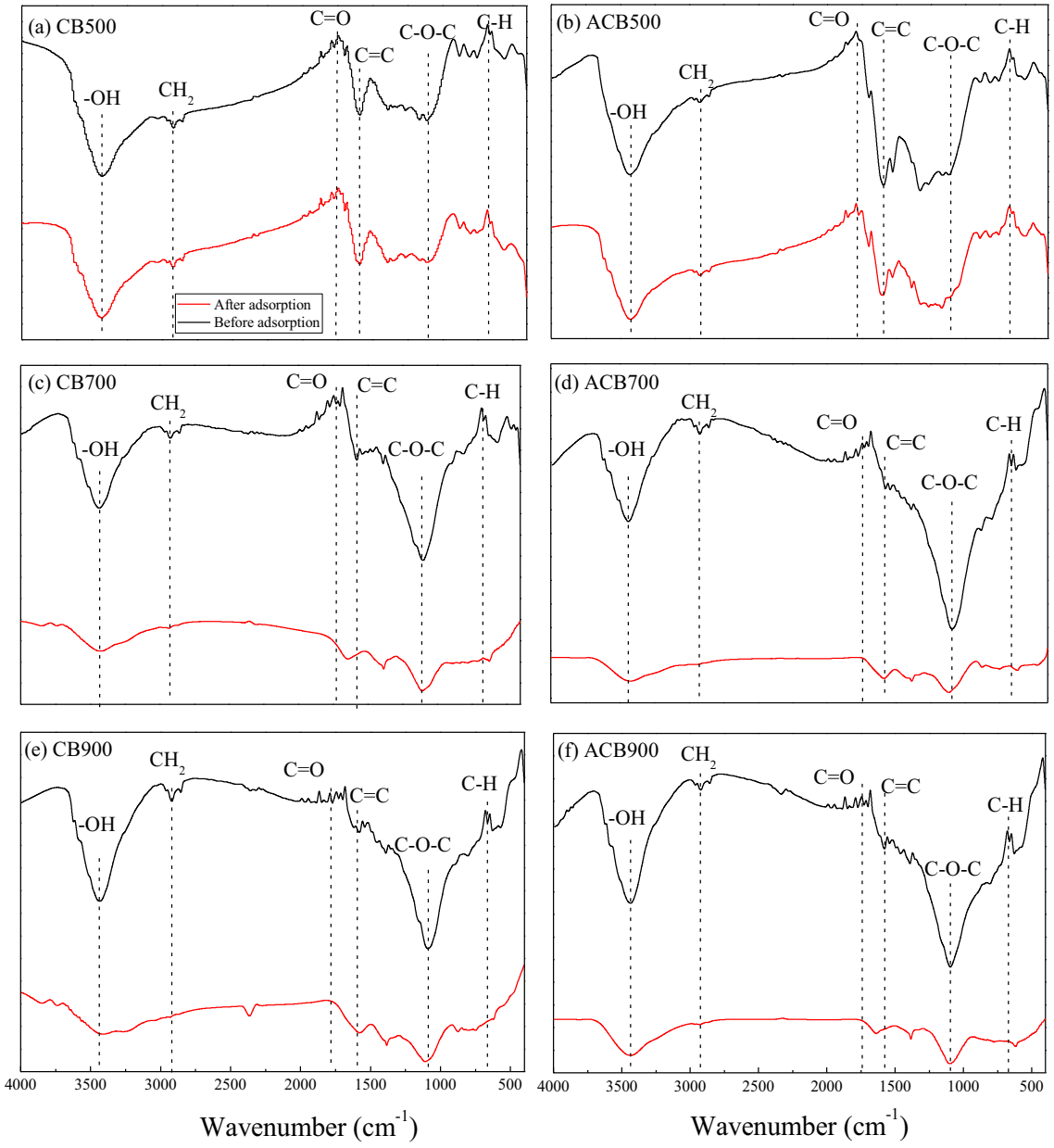


**Fig. 6.** FTIR spectra of fresh and oxidized biochars before and after PSNPs adsorption.

groups) and C═O (quinones carbonyl groups) for ACB900 and 13.49% and 8.97% for CB900 respectively. These changes were associated with H-bonding and involvement of O-containing functional groups in the adsorption of PSNPs to biochar.

### 3.7. Adsorption mechanisms

To compare the adsorption performances and study the adsorption mechanism of different samples, the $Q_{max}$ (extracted from the Langmuir adsorption isotherms at a constant PSNPs equilibrium concentration of 1 g/L) were correlated with various properties of the samples, including molar ratio of H/C, O/C, (N + O)/C, and surface area (Fig. S7). Generally, the value of $Q_{max}$ was negatively correlated for fresh biochar with H/C, O/C, (N + O)/C and was positively correlated with the surface area, whereas the $Q_{max}$ of oxidized biochar was negatively correlated with H/C, positively correlated with O/C, and (N + O)/C and with the surface area (Fig. S7). Concerning the samples generated at different pyrolysis temperatures and after oxidation, the reason causing the increase of adsorption capacity is distinctive. For the fresh biochar, the $Q_{max}$ value increased from CB500-CB900 mainly due to the increase of aromaticity (H/C), hydrophobicity, and the increase in surface area (Table 1, Fig. S7). The increase of temperature leads to increased hydrophobicity, aromaticity, and surface area, resulting in high adsorption for PSNPs particles. For the oxidized biochar, the $Q_{max}$ value also increased from ACB500 to ACB900 and was higher than those for fresh ones. The increase of $Q_{max}$ can be mainly ascribed to the considerable increase of surface area, as well as to the increase of aromaticity and surface oxygen containing groups.

The above results show that, the increase of surface area is probably the major factor that explains the increase of PSNPs adsorption considering both the pyrolysis temperature and oxidation. However, hydrophobic interaction might have played a more important role in PSNPs adsorption to fresh biochar, whereas the oxygen containing surface groups could be more involved in the PSNPs adsorption to oxidized

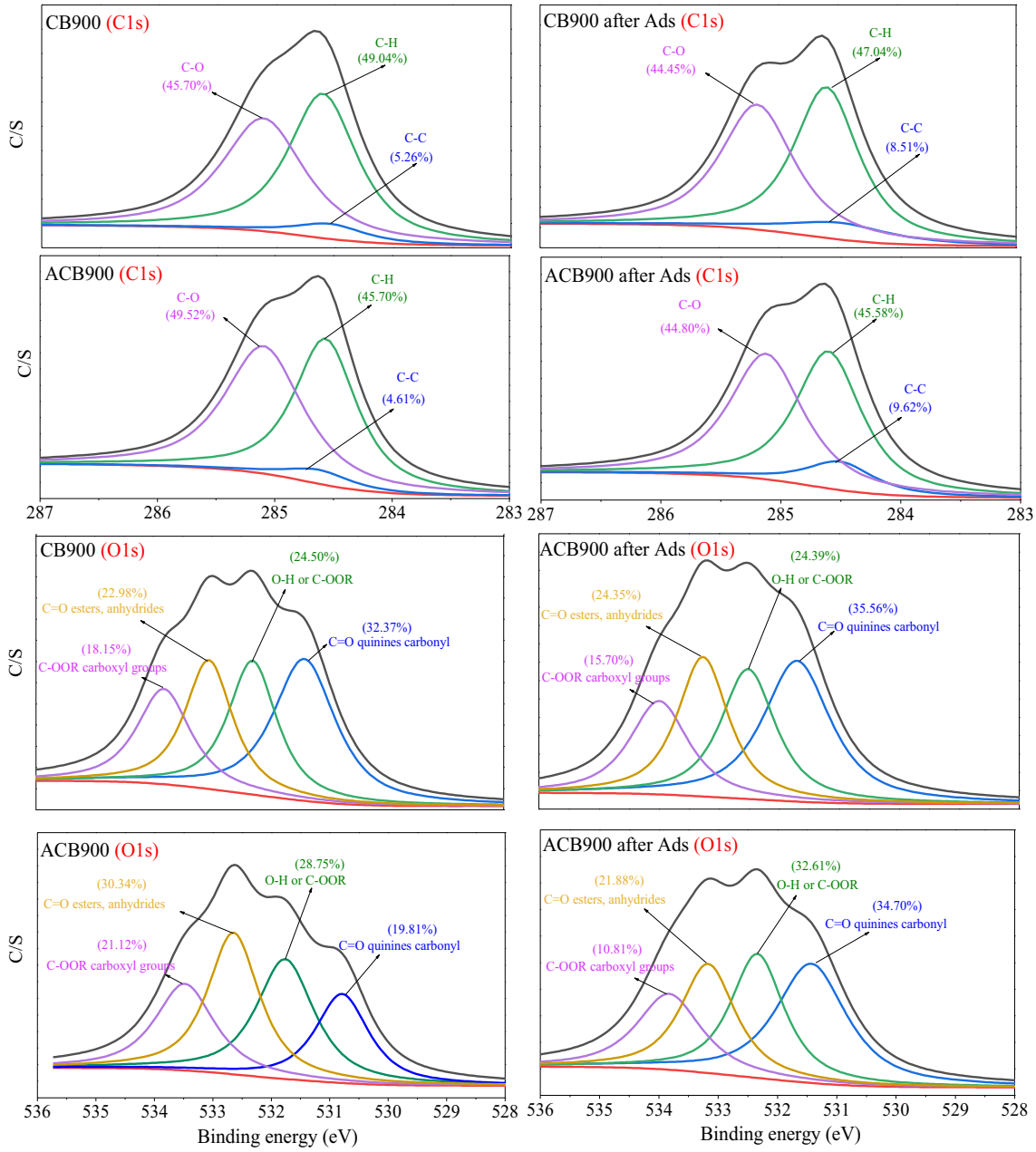


**Fig. 7.** Fitted curves for C1s and O1s spectra of biochars before and after PSNPs adsorption.

biochar. Oxygen containing groups can form hydrogen bonding with surface groups on PSNPs and the FTIR and XPS spectra support these suggestions. The pore filling may have also played a role in PSNPs adsorption to biochar. Apart from these attractive forces, electrostatic repulsion also plays an important role in the adsorption between the surface of biochars and PSNPs, as shown in the pH dependency of PSNPs adsorption to both the fresh and oxidized biochar and the DLVO analysis discussed above. Similarly, Tong et al. (2020) demonstrated that less electrostatic repulsion existed between the quartz sands with $Fe_3O_4$-biochar amendment and plastic particles, which resulted in more effective retention of plastic particles in the sand columns with the addition of $Fe_3O_4$-biochar than biochar alone. But the results from the $N_2$ adsorption method can't explain clearly, because the $N_2$ data give only the micropore size of biochar (<100 nm). So, we analysed the pore size with the mercury porosimeter method (>100 nm). As shown in Fig. S4, all the biochar (fresh and oxidized) showed the peak at the same place (2246.92 nm), indicating that all the biochar can adsorb PSNPs (45.0–48.0 nm) through pore filling. Similar result has been observed previously with regard to the pore filling on micro/nanoplastic adsorption to biochar (Wang et al., 2020). But pore filling can't explain the difference adsorption between fresh and oxidized biochar. However, the involvement of these mechanisms is challenging to qualify.

## 4. Conclusion

In this study, the adsorption of PSNPs to fresh and oxidized ($HNO_3$/$H_2SO_4$) corncob biochar produced at varied pyrolysis temperatures was investigated. The adsorption capacity was enhanced for biochar with the increase of pyrolysis temperature and after oxidation. The increase of PSNPs adsorption could largely be explained by the increase of specific surface area, but the increase of adsorption and surface area

was not proportional. One reason of this non-proportional change could be attributed to the creation of pores smaller than the size of PSNPs particles (50 nm). Other reasons could be attributed to the difference of surface properties of biochars. The physical and chemical properties of biochar samples, significantly influenced by the pyrolytic temperature and oxidation, play a crucial role in the adsorption of PSNPs. Hydrophobic interaction and hydrogen bonding may have been involved in PSNPs adsorption to both the fresh and oxidized biochars. However, hydrophobicity interactions might be more important in PSNPs adsorption to fresh biochars than to oxidized biochars, whereas for oxidized biochars hydrogen bonding involving oxygen containing groups seemed more important than for fresh biochars. The PSNPs adsorption to both the fresh and oxidized biochar decreased in general with the increase of pH. At higher pH, electrostatic repulsion increased, which reduced adsorption.

The current work showed the adsorption ability of biochar for PSNPs and the potential enhancement of adsorption during the aging process of biochar. These findings will benefit further studies to explore the possibilities of using biochar to sequester nanoplastics in the natural environment.

## CRediT authorship contribution statement

**Abdoul Salam Issiaka Abdoul Magid:** Adsorption material preparation, methodology, laboratory experiment performance, formal analysis, and writing original draft. **Md. Shafiqul Islam:** Adsorption material preparation, laboratory experiment performance, formal analysis, writing-review and editing. **Yali Chen:** Conceptualization, methodology, writing-review and editing, funding acquisition. **Liping Weng:** Conceptualization, methodology, writing-review and editing. **Jinbo Li:** Writing-review and editing. **Jie Ma:** Writing-review and editing. **Yongtao Li:** Writing-review and editing. All authors contributed substantially to revisions.

## Declaration of competing interest

The authors declare that they have no known competing financial interests or personal relationships that could have appeared to influence the work reported in this paper.

## Acknowledgements

This research is supported by the National Natural Science Foundation of China (41701355), the National Key Research and Development Program of China (2017YFD0801003) and Central Public-interest Scientific Institution Basal Research Fund (2020-jbkyywf-mj).

## Appendix A. Supplementary data

Supplementary data to this article can be found online at https://doi.org/10.1016/j.scitotenv.2021.147115.

## References

Ahmad, M., Lee, S.S., Dou, X., Mohan, D., Sung, J.K., Yang, J.E., Ok, Y.S., 2012. Effects of pyrolysis temperature on soybean stover- and peanut shell-derived biochar properties and TCE adsorption in water. Bioresour. Technol. 118, 536–544. https://doi.org/10.1016/j.biortech.2012.05.042.

Ahmad, M., Rajapaksha, A.U., Lim, J.E., Zhang, M., Bolan, N., Mohan, D., Vithanage, M., Lee, S.S., Ok, Y.S., 2014. Biochar as a sorbent for contaminant management in soil and water: a review. Chemosphere 99, 19–33. https://doi.org/10.1016/j.chemosphere.2013.10.071.

Alhashimi, H.A., Aktas, C.B., 2017. Life cycle environmental and economic performance of biochar compared with activated carbon: a meta-analysis. Resour. Conserv. Recycl. 118, 13–26. https://doi.org/10.1016/j.resconrec.2016.11.016.

Andrady, A.L., 2011. Microplastics in the marine environment. Mar. Pollut. Bull. 62, 1596–1605. https://doi.org/10.1016/j.marpolbul.2011.05.030.

Angst, T.E., Patterson, C.J., Reay, D.S., Anderson, P., Peshkur, T.A., Sohi, S.P., 2013. Biochar diminishes nitrous oxide and nitrate leaching from diverse nutrient sources. J. Environ. Qual. 42, 672–682. https://doi.org/10.2134/jeq2012.0341.

ASTM International, 1984. Standard test method for chemical analysis of wood charcoal - designation: D 1762 – 84 (reapproved 2001). Annu. B. ASTM Stand. 84, 292–293. https://doi.org/10.1520/D1762-84R07.2.

Bergendahl, J., Grasso, D., 1999. Prediction of colloid detachment in a model porous media: thermodynamics. AICHE J. 45, 475–484. https://doi.org/10.1002/aic.690450305.

Bläsing, M., Amelung, W., 2018. Plastics in soil: analytical methods and possible sources. Sci. Total Environ. 612, 422–435. https://doi.org/10.1016/j.scitotenv.2017.08.086.

Bogusz, A., Oleszczuk, P., Dobrowolski, R., 2015. Application of laboratory prepared and commercially available biochars to adsorption of cadmium, copper and zinc ions from water. Bioresour. Technol. 196, 540–549. https://doi.org/10.1016/j.biortech.2015.08.006.

Cao, X., Ma, L., Liang, Y., Gao, B., Harris, W., 2011. Simultaneous immobilization of lead and atrazine in contaminated soils using dairy-manure biochar. Environ. Sci. Technol. 45, 4884–4889. https://doi.org/10.1021/es103752u.

Chee, J., Yeo, C., Muiruri, J.K., Thitsartarn, W., Li, Z., 2017. Recent advances in the development of biodegradable PHB-based toughening materials: approaches , advantages and applications. Mater. Sci. Eng. C 92, 1092–1116. https://doi.org/10.1016/j.msec.2017.11.006.

Chen, M., Xu, P., Zeng, G., Yang, C., Huang, D., Zhang, J., 2015. Bioremediation of soils contaminated with polycyclic aromatic hydrocarbons, petroleum, pesticides, chlorophenols and heavy metals by composting: applications, microbes and future research needs. Biotechnol. Adv. 33, 745–755. https://doi.org/10.1016/j.biotechadv.2015.05.003.

Cho, H., Wepasnick, K., Smith, B.A., Bangash, F.K., Fairbrother, D.H., Ball, W.P., 2010. Sorption of Aqueous Zn[II] and Cd[II] by Multiwall Carbon Nanotubes: the relative roles of oxygen-containing functional groups and graphenic carbon. Am. Chem. Soc. 26, 967–981. https://doi.org/10.1021/la902440u.

Creamer, A.E., Gao, B., Zhang, M., 2014. Carbon dioxide capture using biochar produced from sugarcane bagasse and hickory wood. Chem. Eng. J. 249, 174–179. https://doi.org/10.1016/j.cej.2014.03.105.

Cross, A., Sohi, S.P., 2011. The priming potential of biochar products in relation to labile carbon contents and soil organic matter status. Soil Biol. Biochem. 43, 2127–2134. https://doi.org/10.1016/j.soilbio.2011.06.016.

Cross, A., Sohi, S.P., 2013. A method for screening the relative long-term stability of biochar. GCB Bioenergy 5, 215–220. https://doi.org/10.1111/gcbb.12035.

Da Costa, J.P., 2019. Nanoplastics in the environment. Environ. Sci. Technol. 47, 82–105. https://doi.org/10.1039/9781788013314-00082.

Da Costa, J.P., Santos, P.S.M., Duarte, A.C., Rocha-santos, T., 2016. (Nano) plastics in the environment – sources , fates and effects. Sci. Total Environ. 566–567, 15–26. https://doi.org/10.1016/j.scitotenv.2016.05.041.

Davranche, M., Veclin, C., Pierson-Wickmann, A.C., El Hadri, H., Grassl, B., Rowenczyk, L., Dia, A., Ter Halle, A., Blancho, F., Reynaud, S., Gigault, J., 2019. Are nanoplastics able to bind significant amount of metals? The lead example. Environ. Pollut. 249, 940–948. https://doi.org/10.1016/j.envpol.2019.03.087.

Duis, K., Coors, A., 2016. Microplastics in the aquatic and terrestrial environment: sources (with a specific focus on personal care products), fate and effects. Environ. Sci. Eur. 28, 1–25. https://doi.org/10.1186/s12302-015-0069-y.

Fan, Q., Sun, J., Chu, L., Cui, L., Quan, G., Yan, J., Hussain, Q., Iqbal, M., 2018. Effects of chemical oxidation on surface oxygen-containing functional groups and adsorption behavior of biochar. Chemosphere 207, 33–40. https://doi.org/10.1016/j.chemosphere.2018.05.044.

Ghaffar, A., Abbas, G., 2016. Adsorption of phthalic acid esters (PAEs) on chemically aged biochars. De Gruyter 5, 407–417. https://doi.org/10.1515/gps-2016-0014.

Ghaffar, A., Saikat, G., Fangfang, L., Xudong, D., Di, Z., Min, W., Hao, L., Bo, P., 2015. Effect of biochar aging on surface characteristics and adsorption behavior of dialkyl phthalates. Environ. Pollut. 206, 502–509. https://doi.org/10.1016/j.envpol.2015.08.001.

Gigault, J., Halle, A. ter, Baudrimont, M., Pascal, P.Y., Gauffre, F., Phi, T.L., El Hadri, H., Grassl, B., Reynaud, S., 2018. Current opinion: what is a nanoplastic? Environ. Pollut. 235, 1030–1034. https://doi.org/10.1016/j.envpol.2018.01.024.

Gupta, G.K., Ram, M., Bala, R., Kapur, M., Mondal, M.K., 2018. Pyrolysis of chemically treated corncob for biochar production and its application in Cr(VI) removal. Environ. Prog. Sustain. Energy 37, 1606–1617. https://doi.org/10.1002/ep.12838.

Han, M., Kangkang, J., Pengfe, J., Ji, Y., Zhou, J., 2017. Bio-butanol sorption performance on novel porous-carbon adsorbents from corncob prepared via hydrothermal carbonization and post-pyrolysis method. Sci. Rep. 7, 1–11. https://doi.org/10.1038/s41598-017-12062-7.

Hassan, M., Liu, Y., Naidu, R., Parikh, S.J., Du, J., Qi, F., Willett, I.R., 2020. Influences of feedstock sources and pyrolysis temperature on the properties of biochar and functionality as adsorbents: a meta-analysis. Sci. Total Environ. 744, 140714. https://doi.org/10.1016/j.scitotenv.2020.140714.

Hurley, R.R., Nizzetto, L., 2018. Fate and occurrence of micro(nano)plastics in soils: knowledge gaps and possible risks. Curr. Opin. Environ. Sci. Health 1, 6–11. https://doi.org/10.1016/j.coesh.2017.10.006.

Ioannidou, O.A., George, S., Zabaniotou, A.A., 2008. Use of biogenic solids for activated carbon via pyrolysis: the case of corn cob. High Temp. Mater. Process. 27, 355–360. https://doi.org/10.1515/HTMP.2008.27.5.355.

Jia, Y., Shi, S., Liu, J., Su, S., Liang, Q., Zeng, X., Li, T., 2018. Study of the effect of pyrolysis temperature on the Cd2+ adsorption characteristics of biochar. Appl. Sci. 8. https://doi.org/10.3390/app8071019.

Jiang, J., Xu, R., Jiang, T., Li, Z., 2012. Immobilization of Cu (II), Pb (II) and Cd (II) by the addition of rice straw derived biochar to a simulated polluted Ultisol. J. Hazard. Mater. 229–230, 145–150. https://doi.org/10.1016/j.jhazmat.2012.05.086.
Jiang, X., Tian, L., Ma, Y., Ji, R., 2019. Quantifying the bioaccumulation of nanoplastics and PAHs in the clamworm Perinereis aibuhitensis. Sci. Total Environ. 655, 591–597. https://doi.org/10.1016/j.scitotenv.2018.11.227.
Jing, F., Sohi, S.P., Liu, Y., Chen, J., 2018. Insight into mechanism of aged biochar for adsorption of PAEs: reciprocal effects of ageing and coexisting Cd2+. Environ. Pollut. 242, 1098–1107. https://doi.org/10.1016/j.envpol.2018.07.124.
Kashiwada, S., 2006. Distribution of nanoparticles in the see-through medaka (Oryzias latipes). Environ. Health Perspect. 114, 1697–1702. https://doi.org/10.1289/ehp.9209.
Kloss, S., Zehetner, F., Dellantonio, A., Hamid, R., Ottner, F., Liedtke, V., Schwanninger, M., Gerzabek, M.H., Soja, G., 2012. Characterization of slow pyrolysis biochars: effects of feedstocks and pyrolysis temperature on biochar properties. J. Environ. Qual. 41, 990–1000. https://doi.org/10.2134/jeq2011.0070.
Koelmans, A.A., Jonker, M.T.O., Cornelissen, G., Bucheli, T.D., Van Noort, P.C.M., Gustafsson, Ö., 2006. Black carbon: the reverse of its dark side. Chemosphere 63, 365–377. https://doi.org/10.1016/j.chemosphere.2005.08.034.
Lee, K.-W., Shim, W.J., Kwon, O.Y., Kang, J.-H., 2013. Size-dependent effects of micro polystyrene particles in the marine copepod Tigriopus japonicus. Environ. Sci. Technol. 47, 11278–11283. https://doi.org/10.1021/es401932b.
Lehmann, J., Joseph, S., 2012. Biochar for environmental management: an introduction. Sci. Technol. 1, 1–12. https://doi.org/10.4324/9781849770552.
Li, Y., Zhou, S., Liu, K., Wang, G., Wang, J., 2020. Application of APCA-MLR receptor model for source apportionment of char and soot in sediments. Sci. Total Environ. 746, 141165. https://doi.org/10.1016/j.scitotenv.2020.141165.
Liu, X., Zhang, Yang, Li, Z., Feng, R., Zhang, Yaozhong, 2014. Characterization of corncob-derived biochar and pyrolysis kinetics in comparison with corn stalk and sawdust. Bioresour. Technol. 170, 76–82. https://doi.org/10.1016/j.biortech.2014.07.077.
Luo, M., Lin, H., Li, B., Dong, Y., He, Y., Wang, L., 2018. A novel modification of lignin on corncob-based biochar to enhance removal of cadmium from water. Bioresour. Technol. 259, 312–318. https://doi.org/10.1016/j.biortech.2018.03.075.
Major, J., Rondon, M., Molina, D., Riha, S.J., Lehmann, J., 2010. Maize yield and nutrition during 4 years after biochar application to a Colombian savanna oxisol. Plant Soil 333, 117–128. https://doi.org/10.1007/s11104-010-0327-0.
María, J., Rosa, de la, Rosado, M., Paneque, M., Miller, A.Z., Knicker, H., 2018. Effects of aging under fi eld conditions on biochar structure and composition: implications for biochar stability in soils. Sci. Total Environ. 613–614, 969–976. https://doi.org/10.1016/j.scitotenv.2017.09.124.
Martin, S.M., Kookana, R.S., Van Zwieten, L., Krull, E., 2012. Marked changes in herbicide sorption-desorption upon ageing of biochars in soil. J. Hazard. Mater. 231–232, 70–78. https://doi.org/10.1016/j.jhazmat.2012.06.040.
Mašek, O., Brownsort, P., Cross, A., Sohi, S., 2013. Influence of production conditions on the yield and environmental stability of biochar. Fuel 103, 151–155. https://doi.org/10.1016/j.fuel.2011.08.044.
Ni, B., Huang, Q., Wang, C., Ni, T., Sun, J., Wei, W., 2019. Competitive adsorption of heavy metals in aqueous solution onto biochar derived from anaerobically digested sludge. ECSN https://doi.org/10.1016/j.chemosphere.2018.12.053.
Nizzetto, L., Futter, M., Langaas, S., 2016. Are agricultural soils dumps for microplastics of urban origin? Environ. Sci. Technol. 50, 10777–10779. https://doi.org/10.1021/acs.est.6b04140.
O'Connor, D., Pan, S., Shen, Z., Song, Y., Jin, Y., Wu, W.M., Hou, D., 2019. Microplastics undergo accelerated vertical migration in sand soil due to small size and wet-dry cycles. Environ. Pollut. 249, 527–534. https://doi.org/10.1016/j.envpol.2019.03.092.
Oss, V., 1993. Acid-base interfacial interactions in aqueous media. Colloids Surf. 78, 1–49. https://doi.org/10.1016/0927-7757(93)80308-2.
Paço, A., Duarte, K., Da Costa, J.P., Santos, P.S.M., Pereira, R., Pereira, M.E., Freitas, A.C., Duarte, A.C., Rocha-Santos, T.A.P., 2017. Biodegradation of polyethylene microplastics by the marine fungus Zalerion maritimum. Sci. Total Environ. 586, 10–15. https://doi.org/10.1016/j.scitotenv.2017.02.017.
Qian, L., Chen, B., 2013. Dual role of biochars as adsorbents for aluminum: the effects of oxygen-containing organic components and the scattering of silicate particles. Environ. Sci. Technol. 47, 8759–8768. https://doi.org/10.1021/es401756h.
Qian, L., Chen, B., 2014. Interactions of aluminum with biochars and oxidized biochars: implications for the biochar aging process. J. Agric. Food Chem. 62, 373–380. https://doi.org/10.1021/jf404624h.
Quevedo, I.R., Tufenkji, N., 2012. Mobility of functionalized quantum dots and a model polystyrene nanoparticle in saturated quartz sand and loamy sand. Environ. Sci. Technol. 46, 4449–4457. https://doi.org/10.1021/es2045458.
Renner, G., Schmidt, T.C., Schram, J., 2018. Analytical methodologies for monitoring micro (nano)plastics: which are fit for purpose? Curr. Opin. Environ. Sci. Heal. 1, 55–61. https://doi.org/10.1016/j.coesh.2017.11.001.
Rossi, G., Barnoud, J., Monticelli, L., 2014. Polystyrene nanoparticles perturb lipid membranes. J. Phys. Chem. Lett. 5, 241–246. https://doi.org/10.1021/jz402234c.
Scheurer, M., Bigalke, M., 2018. Microplastics in Swiss floodplain soils. Environ. Sci. Technol. 52, 3591–3598. https://doi.org/10.1021/acs.est.7b06003.
Schwaferts, C., Niessner, R., Elsner, M., Ivleva, N.P., 2019. Methods for the analysis of submicrometer- and nanoplastic particles in the environment. TrAC - Trends Anal. Chem. 112, 52–65. https://doi.org/10.1016/j.trac.2018.12.014.
Shang, L., Nienhaus, K., Nienhaus, G.U., 2014. Engineered nanoparticles interacting with cells: size matters. J. Nanobiotechnology 12, 1–11. https://doi.org/10.1186/1477-3155-12-5.
Shen, Z., Zhang, J., Hou, D., Tsang, D.C.W., Sik, Y., Alessi, D.S., 2018. Synthesis of MgO-coated corncob biochar and its application in lead stabilization in a soil washing residue. Environ. Int. 122, 357–362. https://doi.org/10.1016/j.envint.2018.11.045.
Sohi, S.P., 2012. Carbon storage with benefits. Science 338, 1034–1035. https://doi.org/10.1126/science.1225987 (80-. ).
Spokas, K.A., 2010. Review of the stability of biochar in soils: predictability of O:C molar ratios. Carbon Manag. 1, 289–303. https://doi.org/10.4155/cmt.10.32.
Steinmetz, Z., Wollmann, C., Schaefer, M., Buchmann, C., David, J., Tröger, J., Muñoz, K., Frör, O., Schaumann, G.E., 2016. Plastic mulching in agriculture. Trading short-term agronomic benefits for long-term soil degradation? Sci. Total Environ. 550, 690–705. https://doi.org/10.1016/j.scitotenv.2016.01.153.
Strungaru, S.A., Jijie, R., Nicoara, M., Plavan, G., Faggio, C., 2019. Micro- (nano) plastics in freshwater ecosystems: abundance, toxicological impact and quantification methodology. TrAC - Trends Anal. Chem. 110, 116–128. https://doi.org/10.1016/j.trac.2018.10.025.
Tan, Z., Yuan, S., Hong, M., Zhang, L., Huang, Q., 2020. Mechanism of negative surface charge formation on biochar and its effect on the fixation of soil Cd. J. Hazard. Mater. 384, 121370. https://doi.org/10.1016/j.jhazmat.2019.121370.
Tong, M., He, L., Rong, H., Li, M., Kim, H., 2020. Transport behaviors of plastic particles in saturated quartz sand without and with biochar/$Fe_3O_4$-biochar amendment. Water Res. 169, 115284. https://doi.org/10.1016/j.watres.2019.115284.
Uchimiya, M., Bannon, D.I., Wartelle, L.H., 2012. Retention of heavy metals by carboxyl functional groups of biochars in small arms range soil. Agric. Food Chemestry 60, 1798–1809. https://doi.org/10.1021/jf2047898.
Wang, Z., Sedighi, M., Lea-langton, A., 2020. Filtration of microplastic spheres by biochar : removal efficiency and immobilisation mechanisms. Water Res. 184, 116165. https://doi.org/10.1016/j.watres.2020.116165.
Wegner, A., Besseling, E., Foekema, E.M., Kamermans, P., Koelmans, A.A., 2012. Effects of nanopolystyrene on the feeding behavior of the blue mussel (Mytilus edulis L.). Environ. Toxicol. Chem. 31, 2490–2497. https://doi.org/10.1002/etc.1984.
Wright, S.L., Kelly, F.J., 2017. Plastic and human health: a micro issue? Environ. Sci. Technol. 51, 6634–6647. https://doi.org/10.1021/acs.est.7b00423.
Wu, J., Jiang, R., Lin, W., Ouyang, G., 2019. Effect of salinity and humic acid on the aggregation and toxicity of polystyrene nanoplastics with different functional groups and charges. Environ. Pollut. 245, 836–843. https://doi.org/10.1016/j.envpol.2018.11.055.
Wu, X., Lyu, X., Li, Z., Gao, B., Zeng, X., Wu, J., Sun, Y., 2020. Transport of polystyrene nanoplastics in natural soils: effect of soil properties, ionic strength and cation type. Sci. Total Environ. 707, 136065. https://doi.org/10.1016/j.scitotenv.2019.136065.
Yang, X., Zhang, S., Ju, M., Liu, L., 2019. Preparation and modification of biochar materials and their application in soil remediation. Appl. Sci. 9, 1365. https://doi.org/10.3390/app9071365.
Zhang, G.S., Liu, Y.F., 2018. The distribution of microplastics in soil aggregate fractions in southwestern China. Sci. Total Environ. 642, 12–20. https://doi.org/10.1016/j.scitotenv.2018.06.004.
Zhang, Y., Luo, Y., Guo, X., Xia, T., Wang, T., Jia, H., Zhu, L., 2020. Charge mediated interaction of polystyrene nanoplastic (PSNP) with minerals in aqueous phase. Water Res. 178. https://doi.org/10.1016/j.watres.2020.115861.